Deposition of porous titanium oxide thin films as anode material for dye sensitized solar cells

Dervaux, Jonathan; Cormier, Pierre-Antoine; Konstantinidis, Stephanos; Di Ciuccio, Riccardo; Coulembier, Olivier; Dubois, Philippe; Snyders, Rony

Published in:
Vacuum

Publication date:
2015

Vacuum 114 (2015) 213–220

Contents lists available at ScienceDirect

Vacuum

journal homepage: www.elsevier.com/locate/vacuum

Deposition of porous titanium oxide thin films as anode material for dye sensitized solar cells

J. Dervaux [a, *], P.-A. Cormier [a], S. Konstantinidis [a], R. Di Ciuccio [b], O. Coulembier [b], P. Dubois [b, c], R. Snyders [a, c]

[a] Chimie des Interactions Plasma Surface, CIRMAP, University of Mons, 23 Place du Parc, B7000 Mons, Belgium
[b] Service des Matériaux Polymères et Composites, CIRMAP, University of Mons, 23 Place du Parc, B7000 Mons, Belgium
[c] Materia Nova Research Center, 1 Avenue Nicolas Copernic, B7000 Mons, Belgium

ARTICLE INFO

Article history:
Received 13 August 2014
Received in revised form
27 October 2014
Accepted 28 October 2014
Available online 4 November 2014

Keywords:
Magnetron sputtering
GLAD
TiO_2
Porous coatings
Photoanodes

ABSTRACT

Crystallized nanoporous TiO_2 thin films were synthesized by combining reactive magnetron sputtering and Glancing Angle Deposition (GLAD). The growth temperature, the bias voltage and the rotation speed of the substrate were studied with the aim to grow nanoporous films presenting anatase constitution which are suitable for Dye Sensitive Solar Cells (DSSC) applications.

By fixing the tilt angle at 85°, we have shown that an increase of the growth temperature up to 450 °C leads to the formation of nanoporous anatase film with a grain size up to 24 nm while by applying a bias voltage leads to a densification of the films as evidenced by scanning electron microscopy and by X-ray diffraction. On the other hand, by rotating the substrate (from 0.1 to 10°/s) during the deposition process, films with larger columns and higher surface roughness (from 45 to 60 nm) were obtained due to an enhanced shadowing effect.

Preliminary dye impregnation experiments have shown that the highest light absorption values are obtained for the films prepared without bias and with no rotation, which is supported by the microstructure of these films presenting the highest porosity. These films, presenting an anatase constitution, are potentially good candidates as an anode in DSSC applications.

1. Introduction

Nowadays, the efficient use of renewable energies represents a major economic and environmental issue. This is obviously also true for the solar energy, by far the most important of them in term of quantity. In this context, among the many advantages of the dye-sensitive solar cells (DSSC), their cheap production cost and good performance at low illumination and high temperatures are very interesting [1–5]. The highest efficiencies [2] are around 10% and, more recently, the fabrication of solid state DSSCs with 15.0% efficiency was announced by Graetzel [6]. Much of the shortfall is due to the poor absorption of low-energy photons by available dyes. Considerable efforts have been made to develop dyes and dye mixtures that absorb better at long wavelengths but, so far, with little success [7]. Another option for improving the absorption of red- and near-infrared light is by thickening the nanoparticle-based film to increase its optical density. This approach is unsuccessful because the film thickness begins to exceed the electron diffusion length through the nanoparticle network [8]. Indeed, the photo-anode of a DSSC is often composed of an array of TiO_2 nano-particles. In the latter situation, the charge transport is limited by trapping–detrapping processes in which both morphological disorder and energy play a role [9]. The structural disorder at the nanoparticle boundaries enhances the scattering of free electrons and thus reduces the electron mobility [10]. So, even if these nanoporous TiO_2 films have large surface areas (around 56 m^2/g for P25 [11]) and allow an efficient collection of photons, the electron transport is a limiting factor for the conversion efficiency. Ideally, the porous film must have interconnected particles, to allow the percolation of the injected electrons [12].

A potential alternative would be a porous crystalline TiO_2 thin film with nanoscale ordered photo-anode architectures, such as nanotubes [12–14], nanorods [15–17] and nanowires [8,18]. The

* Corresponding author. Tel.: +32 65554945; fax: +32 554941.
E-mail addresses: Jonathan.Dervaux@umons.ac.be (J. Dervaux), Pierre-Antoine.Cormier@umons.ac.be (P.-A. Cormier), Sephanos.Konstantinidis@umons.ac.be (S. Konstantinidis), Riccardo.diciuccio@umons.ac.be (R. Di Ciuccio), Olivier.Coulembier@umons.ac.be (O. Coulembier), Philippe.Dubois@umons.ac.be (P. Dubois), Rony.Snyders@umons.ac.be (R. Snyders).

http://dx.doi.org/10.1016/j.vacuum.2014.10.016
0042-207X/

main potential advantage of these structures relies on a better collection of charges as they provide a more direct path towards the external circuit so that recombination at the boundary grains and exposure to the electron acceptors in the electrolyte is avoided. In this way, faster transport and a slower recombination rate lead to a minimization of charge losses. However, the synthesis of these porous materials by sol-gel method [8,19], anodic oxidation [20], or, electron beam evaporation [21], usually leads to amorphous structures which require additional annealing treatments to crystallize TiO_2 films.

The crystalline constitution of TiO_2 is also important in order to optimize the charge separation and transport in a DSSC. The anatase phase of TiO_2 is usually preferred as the electron acceptor in DSSCs, partly due to the difference in the band-gap value of anatase and rutile TiO_2 polymorphs. The anatase conduction band is 0.2 V more negative than that of rutile, a larger maximum photovoltage can be thus obtained for anatase (assuming that the same redox mediator is employed) [22,23]. Nevertheless, it has been shown that a mixture of rutile and anatase TiO_2 crystals could enhance the photo-current and the overall solar conversion efficiency [24]. In this work, the best photo-current and overall solar conversion efficiency were obtained for a rutile content in the film around of 13% by weight. This was explained by a synergistic effect between anatase and rutile crystal. Interfacial electron transfer occurs from rutile to anatase: photo-excited electrons injected into rutile can be transferred to the conduction-band of anatase [24]. With anatase and rutile in close contact, photo-excited electrons and holes are preferentially trapped in the anatase and the rutile phases inhibiting the detrimental electron–hole recombination [25]. However, the increase of the rutile concentration above this percentage appears to be detrimental to the DSSCs because the diffusion coefficient of conduction-band electrons in rutile is significantly smaller than that in anatase [26].

In order to generate such a porous coating while controlling the phase constitution, we combined Reactive Magnetron Sputtering (RMS) and Glancing Angle Deposition (GLAD). The magnetron sputtering process allows precise control of the microstructure and related properties of the film such as its density, adhesion, surface roughness and crystallinity and it is also cost effective for industrial applications, overcoming the current barriers in other film deposition processes [27]. Anatase TiO_2 thin films have already been grown successfully at room temperature on glass substrates using dc magnetron sputtering in reactive mode [28]. The crystallization of TiO_2 films at room temperature is mainly promoted by energetic particle bombardment (electrons, atoms, ions, molecules and even charged clusters) during sputtering. It has been demonstrated that deposition parameters have great impact on the properties of these films. Indeed, a sputtered thin film which is crystallized by a supply of energy will be dense and therefore the use of GLAD is necessary in this case. Ballistic shadowing is the foundation of GLAD-based thin film engineering. Such shadowing is only possible if the incoming vapour flux is well collimated. In this method, the substrate can be tilted with an angle (α) and/or rotated with an angle (φ) step by step or with a continuous angular speed (φ_s) in order to generate a columnar porous thin film (Fig. 1). The GLAD process enables the growth of columnar thin films with specially engineered nanostructures. These films are extremely porous and consist of isolated columns that can take the form of, for example, helices, vertical posts and polygonal spirals [29]. The porosity (inter-columnar space) and the columnar tilt angle (β) can be tuned to have open pores (mesopores) to increase the specific surface area and improve the dye and electrolyte penetration in the case of specific DSSC applications [30,31].

The combination of MS and GLAD techniques have already been used to synthesize nanostructured thin films comprising different

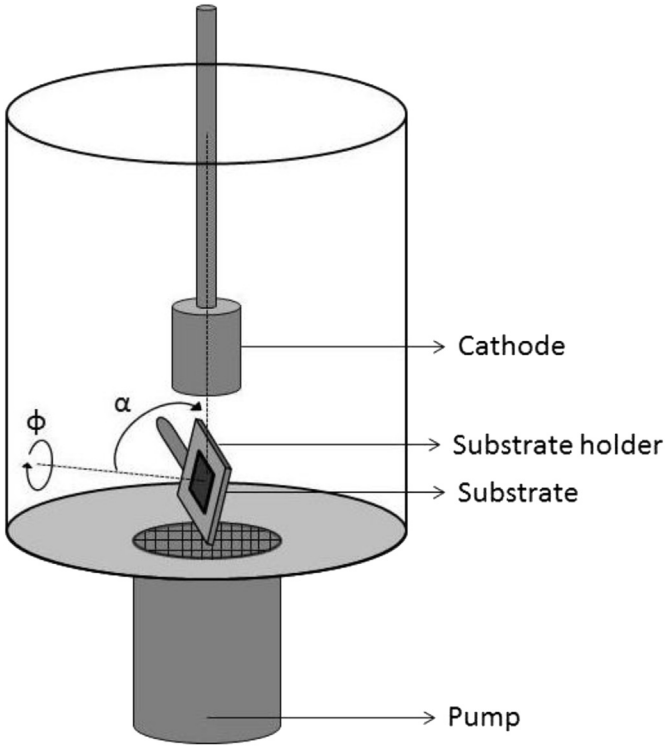

Fig. 1. Experimental setup diagram of the deposition chamber.

types of materials such as chromium [32,33], titanium [34–36], and titanium dioxide [37,38]). Z. Michalčík et al. [37] prepared TiO_2 thin films by the MS and GLAD methods in order to increase the photocatalytic activity. Their nanostructured films were characterized by a higher surface roughness and a substantially higher relative specific surface compared with films prepared by conventional MS. For the application of the anatase films as photo-anodes in dye-sensitized solar cells, Su-Il In et al. [38] prepared vertically aligned anatase TiO_2 nanowire arrays on FTO (Fluorine doped Tin Oxide) coated glass substrates via pulsed DC MS at low temperature. They found a preliminary photo-conversion efficiency of 1.07% for their nanowire-based photo-anode 3.6 μm thick. This is slightly more efficient than single crystals or flat electrodes of polycrystalline films of tin-oxide or titanium-oxide used like a photo anode. In spite of the efficient electron injection into the semiconductor, the light harvesting efficiency was very small and the efficiencies of the solar cells were extremely low (below 1%) [39,40]. Nanostructures, such as vertically aligned nanowires, provide direct pathways for electron transport and, when used as photo electrodes, improve the electron diffusion-length, electron life-time and diffusion-coefficient. However, they have a fundamental disadvantage: they do not provide the necessary specific surface area for dye adsorption, resulting in DSSCs with poor efficiencies. Therefore, in this work, the interrelated and nonlinear parameters of both MS and GLAD were varied in order to determine an experimental window allowing the growth of porous TiO_2 films presenting an anatase and/or rutile crystalline structure that allow significant grafting of dye molecules, which were a conjugated polymer, namely regioregular poly(3-hexylthiophene, P3HT), in this work.

Conjugated polymers are a special class of material gathering the advantages of plastics and semiconductor properties [41]. The conjugated double-bonds in the main chain can interact with light and determine the optoelectronic properties of the polymers [42,43]. Among conjugated polymers, P3HT is of major interest

[43–45] for its high hole mobility, absorption in the visible range, good solubility in organic solvents, low toxicity and chemical and thermal stability.

The crucial point is the incompatibility between the hydrophilic surface of the metal oxide and the hydrophobic nature of the conjugated polymer. The segregation phase between both organic and inorganic components, in fact, reduces the interface between the donor and acceptor materials and, consequently, the charge-transfer efficiency (4). Groups with carboxylic acid functions conjugated to the polymer improve the interactions at the interface polymer-inorganic substrate, increasing the photo-induced electron transfer [46].

2. Experimental details

All experiments were carried out in a cylindrical stainless steel chamber (height: 60 cm, diameter: 42 cm). The chamber was evacuated by a turbo-molecular pump (Edwards nEXT400D 160W), backed by a dry primary pump, down to a residual pressure of 10^{-4} Pa.

An unbalanced magnetron cathode was installed at the top of the chamber facing the substrate at a distance of 80 mm (Fig. 1). A 2-inch in diameter and 0.25-inch thick Ti target (99.99% purity) was used. The target was sputtered in DC mode using an Advanced Energy MDK 1.5 K power supply. A mixture of argon (8 sccm) and oxygen (2 sccm) was injected in the chamber in order to grow stoichiometric TiO_2 film (poisoned regime). Conductive silicon wafers (100) and Indium tin oxide (ITO) coated glasses were used as substrates, cleaned with detergent (RBS) solution and rinsed with ultra-pure water. ITO-coated glass is the substrate that will be used in the DSSC stack and it was used here to characterize the absorption in the UV–visible range. The substrates were tilted to $\alpha = 85°$ with respect to the cathode axis in order to induce ballistic shadowing and consequently the growth of nanostructured films.

The rotation speed (φ_s), the bias voltage (U_b) and the substrate temperature (T_s) were varied in order to study their influence on the thin film properties. The different values utilized are reported in Table 1. The total pressure and the sputtering power were kept constant at 0.1 Pa and 150 W, respectively. The deposition rate measured by profilometry is 2 ± 0.4 nm/min for these conditions and is reduced by a factor of approximately 2 when biasing or rotating the substrate. The substrate temperature has no influence on the rate.

The phase constitution was determined by Grazing Incidence X-ray Diffraction (GIXRD) analysis (Panalytical Empyrean) with a Cu Kα 1 source (1.5406 Å) and 8046 keV. The X-ray source voltage was fixed at 45 kV and the current at 40 mA. The Scherrer equation was used to evaluate the grain size. The morphology was characterized with a field emission gun scanning electron microscope (FEG-SEM Hitachi SU8020). In order to compare the films, their thickness was kept constant at 230 ± 20 nm. The latter was measured by a Dektak 150 profilometer. An AFM Bruker Multimode microscope with Nanoscope IIIa Controller (Etched Si probes (Ref. PPP-NCHR, Nanosensors GmbH)) was used to determine the root mean square (RMS) roughness over a 5 μm^2 surface by an average peak-valley height.

Table 1
Deposition process parameters with their variation range.

Parameters	Variation range
Bias voltage (U_b)	0, −50, −100, −150, −200 V
Substrate temperature (T_s)	100, 250, 350, 450 °C
Rotation speed (φ_s)	0.1, 1.0, 10 °/s

Finally, the TiO_2 surface was grafted with a dye by dip coating using a 10 mg per ml solution of P3HT-COOH (with ~30 thiophene units) in chloroform. The films were then rinsed with chloroform to remove ungrafted P3HT-COOH molecules. To characterize the adsorption of the dye on the TiO_2, the optical absorption of the thin film before and after grafting was measured by using a UV–visible spectrophotometer (UV–VIS–NIR Cary G5) in the 350–800 nm wavelength range.

The regioregular polymer Br-P3HT-H ($M_{n,GPC} = 5400$ g/mol; $Đ_M$ 1.08) was achieved by GRIM polymerization [47–50]. The aldehyde functionalization was realized by Vilsmeier–Haack reaction [51,52] followed by a Witting reaction [46]. The 4-((bromo-triphenylphosphoranyl) methyl)benzoic acid useful for the Wittig reaction was synthesized in accord to the state-of-the-art [53].

3. Results

A preliminary study aiming to determine the experimental window in which the deposition rate was reasonably high allowed the determination of the following deposition conditions: 0.1 Pa, 150 W and $\alpha = 85°$, which have been considered as the reference conditions for this work. Therefore these parameters were kept constant for all experiments. Typical film structure as obtained in these conditions is presented in Fig. 2.

A fibrous columnar structure which is typical of sputtered thin film could be observed. This structure corresponds to the Zone 1 in the Structure Zone Model of Thornton [54]. The structure of vapour-deposited coatings grown under these conditions is typically columnar, characterized by voided open boundaries, and is superimposed on a microstructure which may be polycrystalline or amorphous. Its occurrence is a fundamental consequence of atomic shadowing acting in concert with the low adatom mobility that characterizes low T/T_m deposition [55]. In our case the shadowing effect was exacerbated by a grazing deposition at $\alpha = 85°$ to generate highly porous thin films with increasing the void between columns.

3.1. Influence of substrate bias

All deposition processes were performed within 180 min. The substrates were not intentionally heated but, due to the sputtering process, the substrate temperature could reach 100 °C as measured by a thermocouple connected to the substrate holder.

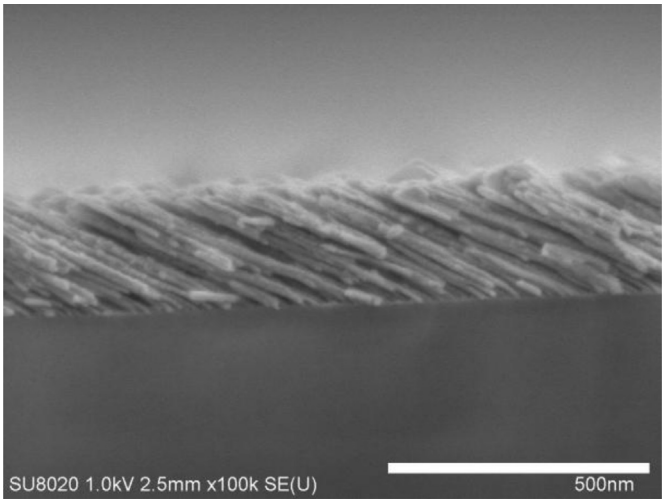

Fig. 2. Cross-section SEM images of TiO_2 nanostructured thin film synthesize in grazing mode ($\alpha = 85°$) at 0.1 Pa and 150 W without substrate bias polarization or heating.

In Fig. 3 the cross-section SEM images of the TiO_2 nanostructured thin films deposited for extreme values of U_b (−50 V and −200 V) are presented. The corresponding morphological characteristics, plotted as a function of U_b (from −50 V to −200 V), are also reported. When applying a substrate bias, the surface is smoothened and the roughness consequently decreases from 30 nm to 10 nm. The width of the columns increases and the inter-columnar space is reduced to zero due to the merging of the columns. The columnar tilt angle (β) increases from 60° to 75° as U_b is varied from 0 V to −50 V and remains fairly constant for higher values. These data could be understood by considering the increase of the ion energy impinging the surface which improves the adatom mobility and is likely to lead to a column merging process but a larger β angle [56] leading to a densification of the films and, therefore, to a decrease of the specific surface area. This is in agreement with previously reported results [57,58]. Sorge and Brett demonstrated by variable angle spectroscopic ellipsometry (VASE) measurements, that films grown at a substrate angle $\alpha = 85°$ show a dramatic increase in density from 0.20 to 0.51 under ion bombardment as the column tilt angle (β) was increased from 44° to 62°. Film density values are normalized relative to that of a film deposited at normal vapour incidence ($\alpha = 0$). It was explained that the open void structure allows better penetration of ions into the pores and enhance the redistribution of surface atoms by sputtering [58].

Fig. 4 shows the X-ray diffraction patterns of the TiO_2 films deposited for different U_b. In addition to the peaks corresponding to Si, anatase and rutile, other peaks are present depending the value of U_b. At 0 V, only the anatase phase was observed with (101), (200), (105) and (211) characteristic peaks [59]. For $U_b = -50$ V, both anatase and the rutile (110) phases are observed. Above −100 V, only the rutile phase is observed. As mentioned before, when U_b increases, the ion energy bombarding the substrate surface increases which allows for the high temperature stable phase of TiO_2, rutile, to be formed at relatively low temperature [60]. Increasing

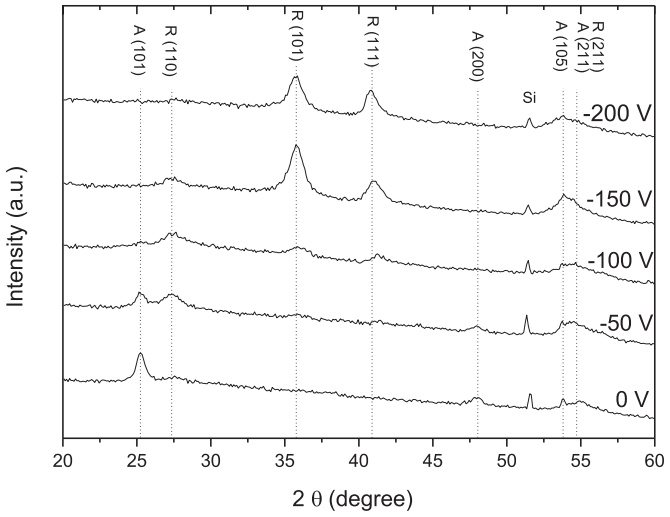

Fig. 4. XRD patterns of the TiO_2 films deposited for different U_b values. A and R denote anatase and rutile phase, respectively.

further the bias voltage to −200 V allows the texture of the rutile phase to change in both (101) and (111) preferential orientations.

Fig. 5 shows how the grain size changes as a function of U_b. Rutile grains are generally smaller (up to 10 nm at −200 V) than anatase grains which could be explained by the fact that anatase is a fast-growing phase in comparison to rutile [60]. The grain size depends strongly on the nucleation rate which can be influenced by the process conditions. Overall, the anatase and rutile grain size becomes larger at a higher deposition U_b due to an enhanced diffusion process on the growing film. From these results it is demonstrated that rutile-containing films can be made even at low

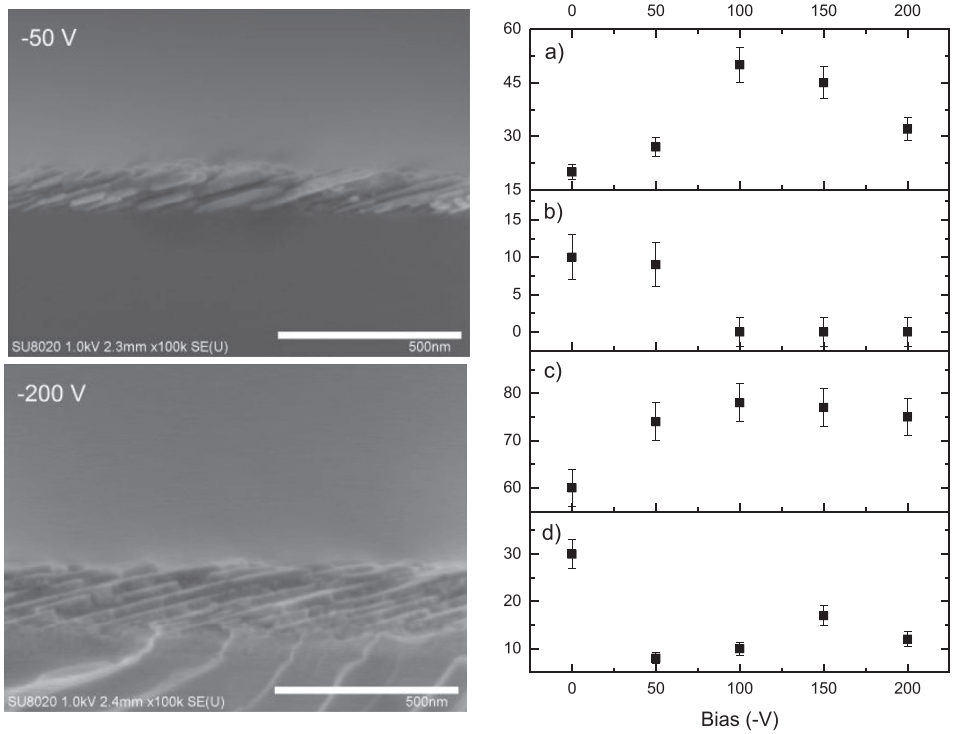

Fig. 3. Cross-section SEM images of TiO_2 nanostructured thin film for extreme values of U_b and the respective morphologies with a) the width of columns (nm), b) the inter-columnar space (nm), c) the columnar tilt β (○) and c) the roughness of the thin film (nm).

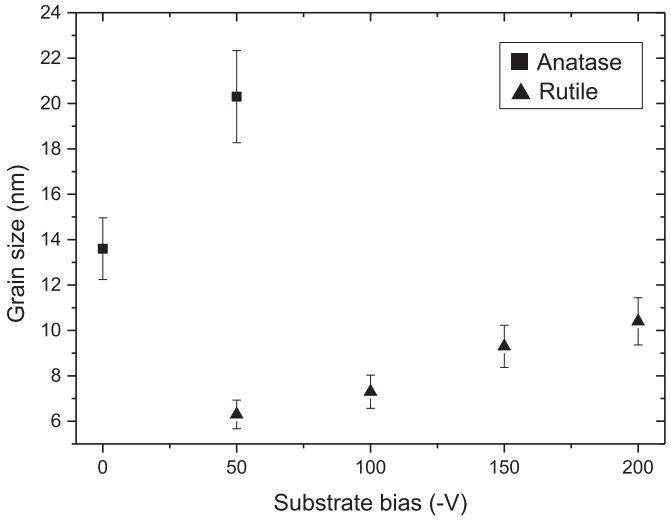

Fig. 5. Grain size of TiO_2 films deposited at different substrate bias voltages.

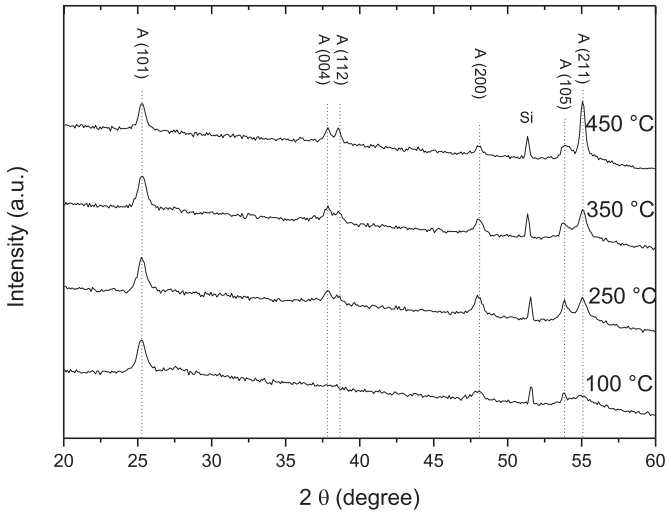

Fig. 7. XRD patterns of the TiO_2 films deposited at different substrate temperatures. A denotes anatase diffraction peaks.

temperatures if the film growth is assisted by ion bombardment. Nevertheless, these films correspond to the less porous structures and are thus characterized by the lowest specific surface area.

3.2. Influence of the substrate temperature

The substrate was heated during the deposition and all other parameters were kept constant as described in the experimental part. The substrate temperature (T_s) ranged from 100 °C to 450 °C. Fig. 6 shows that the roughness and the columnar tilt are not significantly affected by T_s and are 30 nm and 60°, respectively. On the other hand, when increasing T_s, the thin columns very close to one another, obtained at low T_s, become larger (from 18 to 42 nm) and more distant from each other; from 10 to 21 nm. These observations are explained considering the effect of T_s on the nucleation processes [61]. An increase in T_s leads to larger and fewer nuclei with a larger spatial separation for the same substrate coverage. The latter implies that a larger area behind an individual nucleus is shadowed. This allows promotion of the growth in the direction towards the flux. Therefore, a smaller number of thicker columns can grow on the substrate surface from the first nuclei [61].

In addition to the microstructural modifications, an increase of T_s is also expected to promote the crystallization of the growing film. The XRD spectra of nanostructured TiO_2 films deposited for different T_s on Si substrates are presented on Fig. 7. All films reveal a dominating (101) anatase crystalline constitution. However, the (211) anatase peak increases with T_s.

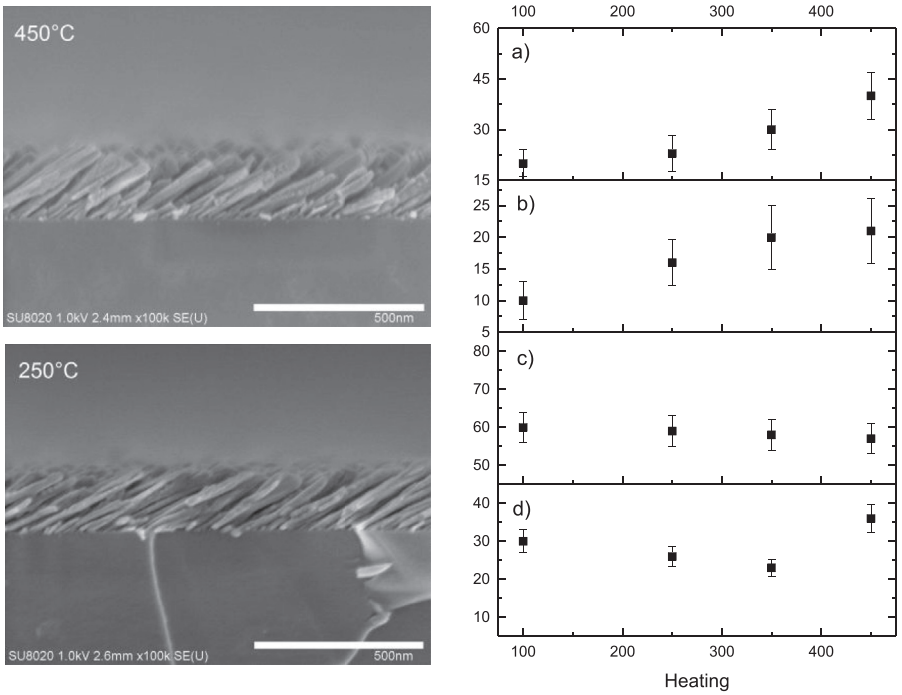

Fig. 6. Cross-section SEM images of TiO_2 nanostructured thin film for extreme values of substrate temperature T_s and the respective morphologies with a) the width of columns (nm), b) the inter-columnar space (nm), c) the columnar tilt β (○) and d) the roughness of the thin film (nm).

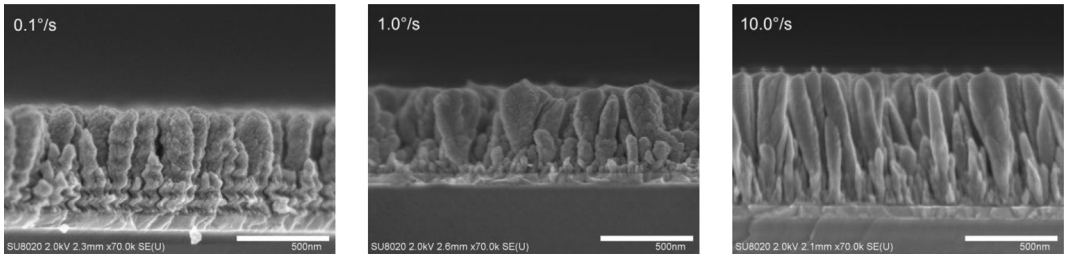

Fig. 8. Cross-section SEM images of nanostructured TiO_2 thin films for three substrate rotation speeds: 0.1, 1.0 and 10°/s.

The (211) anatase orientation has larger grain size than the (101) orientation. This is why the global value of the grain size increases from 13 to 24 nm (not shown here) for $T_s = 450$ °C which is consistent with previous studies [60,62].

3.3. Influence of substrate rotation speed

The rotation speed was varied ($\varphi_s = 0.1, 1.0$ and 10°/s) keeping all other parameters constant. In order to grow crystallized nanostructured TiO_2 films with large open pores, all depositions were performed while heating the substrate at 450 °C and without bias. All films present an anatase crystalline constitution.

Fig. 8 shows the SEM pictures of the cross-sectional views of TiO_2 films synthesized with three angular substrate rotation speeds (φ_s) increasing from 0.1 to 10.0 °/s. The pictures reveal vertical columns characterized by a significant roughness, from 44.5 to 59.3 nm for 0.1 and 10°/s, respectively. With increasing φ_s, the number of turns of the helical column increase proportionally, resulting in an elongated morphology of the column and a decrease of the film porosity due to the self-shadowing effect [63]. Thus, the helical pitch (the height of one "turn" of a helix) may be varied by choosing the rotation speed.

This microstructure is explained as follows: the growth process starts with the development of single spiral fibres. As the growth continues, those fibres eventually merge to form broader structures. In this case, the substrate temperature fixed at 450 °C leads to the merging of the first helicoidal structures due to the increased diffusion rate of the adatoms. This observation is in agreement with previously published studies [64] which have shown that the surface diffusion has a strong impact on i) the merging behaviour of nanospirals, ii) the diameter of single nanostructure features and iii) overall density of the deposited film. At high rotation speed, the helical pitch becomes very small and, ultimately, if the helical pitch is less than the characteristic surface adatom diffusion length, the helix degenerates into a straight vertical pillar. The vertical columns arise because of the rapid rotation speed of the substrate, which allows the particle flux to arrive evenly from all angles φ so the columns will not grow preferentially in any given direction [34].

3.4. Dye adsorption efficiency

The adsorption efficiency of the P3HT-COOH dye on the nanostructured TiO_2 films has been evaluated using UV–visible absorption. The experimental conditions leading to TiO_2 films with the highest porosity, i.e. highest inter columnar space, were chosen. Indeed, this is expected to provide a high specific surface area and thus enhance the adsorption and the surface coverage efficiency of the dye i.e. the number of P3HT-COOH molecules that are adsorbed. A TiO_2 film was therefore deposited on ITO glass (necessary for the absorption measurements) using the following conditions: 0.1 Pa, 150 W during 240 min with $\alpha = 85°$, $\varphi_s = 0°/s$ and $T_s = 450$ °C. Our data demonstrates that the use of an ITO covered glass substrate did not influence significantly the properties of the deposited films. As an example, the cross-section SEM image is presented in Fig. 9a which is completely comparable to the one reported on the Si wafer in Fig. 6. As expected the film exhibits large open pores. A TiO_2 film was deposited with the same experimental conditions but using $\alpha = 0°$. This was also evaluated in terms of dye absorption for comparison since the film is dense and does not present observable porosity as shown in Fig. 9b.

The UV–visible absorption spectra, of both dye sensitized TiO_2 films, are shown on Fig. 10 on which it appears that the absorption of light is significantly higher; by one order of magnitude on the nanostructured TiO_2 film. The maximum of absorption is located around $\lambda = 500$ nm corresponding to the maximum absorption wavelength of the P3HT-COOH molecule [46]. This increased absorption is clearly observable with the naked eye (Fig. 10).

Table 2 reports the relative intensities of the dye absorption peak at 500 nm for other TiO_2 thin films. It can be seen that heating the substrate during the growth does not affect the dye absorption while increasing the bias and the rotation speed reduce it dramatically. These data are perfectly correlated to the microstructure of the films which is much denser when biasing or rotating the substrate.

Overall when considering the need to crystallize the material for a use as an anode in DSSC, the thin films synthesized using $T_s = 450$ °C are the best candidates.

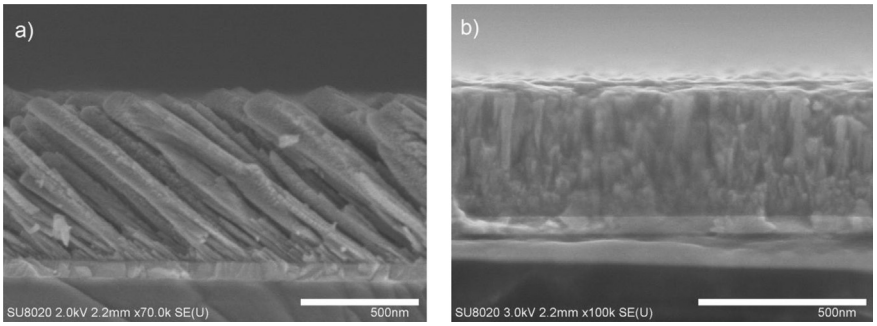

Fig. 9. Cross-section SEM images of TiO_2 a) nanostructured thin film and b) plane (non-structured) thin film synthesized on ITO-coated glass substrates at 450 °C.

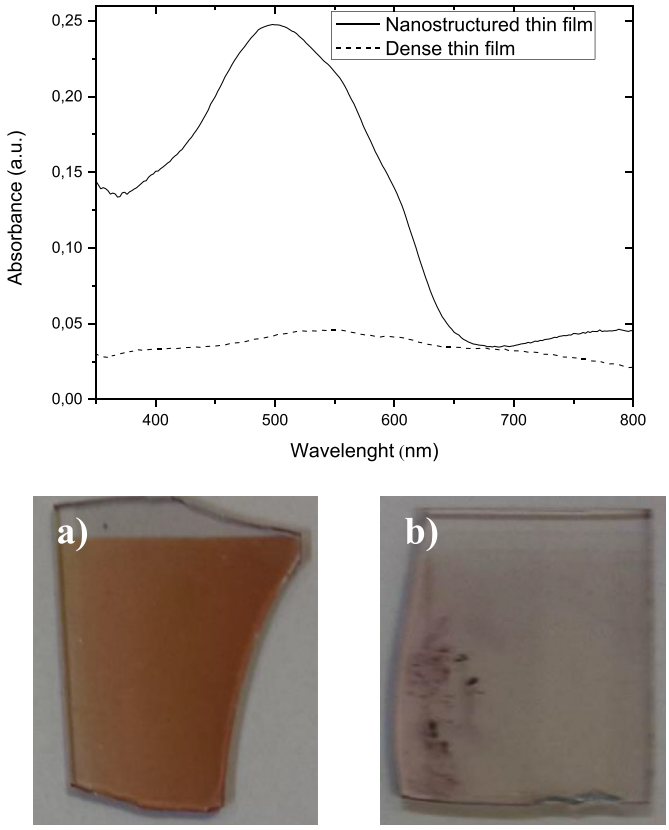

Fig. 10. UV–visible absorption spectra of dye sensitized TiO_2 nanostructured a) and plane thin film b) along with the corresponding pictures.

4. Conclusions

TiO_2 thin films were prepared by combining GLAD ($\alpha = 85°$) and reactive DC magnetron sputtering in order to obtain nanostructured and crystallized thin films which may be used as the photo-anode in DSSCs. The effect of the substrate bias voltage, the substrate temperature, and the substrate rotation speed on the TiO_2 film microstructure and crystalline constitution has been investigated.

It has been observed that, when applying a bias voltage, the phase constitution of TiO_2 films can be controlled from pure anatase to pure rutile films. Nevertheless, the use of the bias leads to a merging of the nano-columns reducing significantly the porosity of the layer which is detrimental for DSSC applications. By heating the substrate, only the anatase phase was observed in the studied range of temperature (from 100 to 450 °C) while the microstructure of the films was not affected and presented a nanoporous structure.

A vertical columnar structure was obtained by rotating the substrate at different speeds. In order to obtain the anatase phase, the substrate temperature was fixed at 450 °C. However, heating the substrate increases the adatom mobility and leads to a merging of the helicoidal structure synthesized at slow rotation speed. At high rotation speed, elongated vertical columns were obtained.

Adsorption efficiency for the dye (P3HT) was evaluated for the different films. The highest absorption has been observed for the film synthesized without bias and without rotation, as expected from the microstructure of the latter. From the present study, we can conclude that heating the substrate at 450 °C, without any substrate rotation, allows a large dye adsorption with an important crystalline domain to be obtained; an essential requirement for an efficient solar cell.

Table 2
Relative intensities of the dye absorption peak at 500 nm with the corresponding deposition conditions at $\alpha = 85°$.

Substrate bias voltage (−V)	Substrate temperature (°C)	Substrate rotation (°/s)	Relative dye absorbed	Crystalline structure
0	RT	0	0.27	A
0	450	0	0.25	A
50	RT	0	0.09	A/R
50	450	0	0.22	A/R
0	450	0.1	0.14	A
0	450	10	0.13	A

Acknowledgements

The authors would like to thank the “Fédération Wallonie-Bruxelles” through the ARC project MADSSCELLS (AUWB-2012-12/17-UMONS N°2) and the Belgian Government through the « Pôle d'Attraction Interuniversitaire » (PAI, P6/08, “Plasma–Surface Interaction”, Ψ). SK is research associate of National Fund for Scientific Research (FNRS – Belgium).

References

[1] Grätzel M. Conversion of sunlight to electric power by nanocrystalline dye-sensitized solar cells. J Photochem Photobiol A Chem 2004;164:3–14.
[2] O'regan B, Grfitzeli M. A low-cost, high-efficiency solar cell based on dye-sensitized. Nature 1991;353:737–40.
[3] Hagfeldt A, Boschloo G, Sun L, Kloo L, Pettersson H. Dye-sensitized solar cells. Chem Rev 2010;110:6595–663.
[4] Nissfolk J, Fredin K, Hagfeldt A, Boschloo G. Recombination and transport processes in dye-sensitized solar cells investigated under working conditions. J Phys Chem B 2006;110:17715–8.
[5] Frank Arthur J, Kopidakis Nikos, Lagemaat Jao van de. Electrons in nanostructured TiO_2 solar cells: transport, recombination and photovoltaic properties. Coord Chem Rev 2004;248:1165–79.
[6] Burschka J, Pellet N, Moon S-J, Humphry-Baker R, Gao P, Nazeeruddin MK, et al. Sequential deposition as a route to high-performance perovskite-sensitized solar cells. Nature 2013;499:316–9.
[7] Renouard T, Fallahpour R-A, Nazeeruddin MK, Humphry-Baker R, Gorelsky S, Lever A, et al. Novel ruthenium sensitizers containing functionalized hybrid tetradentate ligands: synthesis, characterization, and INDO/S analysis. Inorg Chem 2002;41:367–78.
[8] Law M, Greene LE, Johnson JC, Saykally R, Yang P. Nanowire dye-sensitized solar cells. Nat Mater 2005;4:455–9.
[9] González-García L, Idígoras J, González-Elipe AR, Barranco A, Anta JA. Charge collection properties of dye-sensitized solar cells based on 1-dimensional TiO_2 porous nanostructures and ionic-liquid electrolytes. J Photochem Photobiol A Chem 2012;241:58–66.
[10] Mor GK, Shankar K, Paulose M, Varghese OK, Grimes CA. Use of highly-ordered TiO_2 nanotube arrays in dye-sensitized solar cells. Nano Lett 2006;6:215–8.
[11] Raj KJA, Viswanathan B. Effect of surface area, pore volume and particle size of P25 titania on the phase transformation of anatase to rutile. Indian J Chem A 2009;48:1378.
[12] Longo C, De Paoli M-A. Dye-sensitized solar cells: a successful combination of materials. J Braz Chem Soc 2003;14:898–901.
[13] Ohsaki Y, Masaki N, Kitamura T, Wada Y, Okamoto T, Sekino T, et al. Dye-sensitized TiO_2 nanotube solar cells: fabrication and electronic characterization. Phys Chem Chem Phys 2005;7:4157–63.
[14] Zhong P, Que W, Liao Y, Zhang J, Hu X. Improved performance in dye-sensitized solar cells by rationally tailoring anodic TiO_2 nanotube length. J Alloys Compd 2012;540:159–64.
[15] Lee BH, Song MY, Jang S-Y, Jo SM, Kwak S-Y, Kim DY. Charge transport characteristics of high efficiency dye-sensitized solar cells based on electrospun TiO_2 nanorod photoelectrodes. J Phys Chem C 2009;113:21453–7.
[16] Kang SH, Choi SH, Kang MS, Kim JY, Kim HS, Hyeon T, et al. Nanorod-based dye-sensitized solar cells with improved charge collection efficiency. Adv Mater 2008;20:54–8.
[17] Xu F, Wu Y, Zhang X, Gao Z, Jiang K. Controllable synthesis of rutile TiO_2 nanorod array, nanoflowers and microspheres directly on fluorine-doped tin oxide for dye-sensitised solar cells. Micro Nano Lett IET 2012;7:826–30.
[18] Cheng C, Fan HJ. Branched nanowires: synthesis and energy applications. Nano Today 2012;7:327–43.
[19] Gan X, Li X, Gao X, Zhuge F, Yu W. ZnO nanowire/TiO_2 nanoparticle photoanodes prepared by the ultrasonic irradiation assisted dip-coating method. Thin Solid Films 2010;518:4809–12.

[20] Zhong P, Que W, Zhang J, Jia Q, Wang W, Liao Y, et al. Charge transport and recombination in dye-sensitized solar cells based on hybrid films of TiO_2 particles/TiO_2 nanotubes. J Alloys Compd 2011;509:7808–13.
[21] Colgan M, Djurfors B, Ivey D, Brett M. Effects of annealing on titanium dioxide structured films. Thin Solid Films 2004;466:92–6.
[22] Cahen D, Hodes G, Grätzel M, Guillemoles JF, Riess I. Nature of photovoltaic action in dye-sensitized solar cells. J Phys Chem B 2000;104:2053–9.
[23] Kavan L, Grätzel M, Gilbert S, Klemenz C, Scheel H. Electrochemical and photoelectrochemical investigation of single-crystal anatase. J Am Chem Soc 1996;118:6716–23.
[24] Li G, Richter CP, Milot RL, Cai L, Schmuttenmaer CA, Crabtree RH, et al. Synergistic effect between anatase and rutile TiO_2 nanoparticles in dye-sensitized solar cells. Dalton Trans 2009:10078–85.
[25] Hurum D, Agrios A, Crist S, Gray K, Rajh T, Thurnauer M. Probing reaction mechanisms in mixed phase TiO_2 by EPR. J Electron Spectrosc Relat Phenom 2006;150:155–63.
[26] Kambe S, Nakade S, Wada Y, Kitamura T, Yanagida S. Effects of crystal structure, size, shape and surface structural differences on photo-induced electron transport in TiO_2 mesoporous electrodes. J Mater Chem 2002;12:723–8.
[27] Window B. Recent advances in sputter deposition. Surf Coatings Technol 1995;71:93–7.
[28] Singh P, Kaur D. Room temperature growth of nanocrystalline anatase TiO_2 thin films by dc magnetron sputtering. Phys B Condens Matter 2010;405:1258–66.
[29] Steele JJ, Brett MJ. Nanostructure engineering in porous columnar thin films: recent advances. J Mater Sci Mater Electron 2007;18:367–79.
[30] González-García L, Parra-Barranco J, Sánchez-Valencia JR, Barranco A, Borrás A, González-Elipe AR, et al. Correlation lengths, porosity and water adsorption in TiO_2 thin films prepared by glancing angle deposition. Nanotechnology 2012;23:205701.
[31] Xie Z, Henry B, Kirov K, Smith H, Barkhouse A, Grovenor C, et al. Study of the effect of changing the microstructure of titania layers on composite solar cell performance. Thin Solid Films 2006;511:523–8.
[32] Lintymer J, Gavoille J, Martin N, Takadoum J. Glancing angle deposition to modify microstructure and properties of sputter deposited chromium thin films. Surf Coatings Technol 2003;174:316–23.
[33] Lintymer J, Martin N, Chappé J-M, Delobelle P, Takadoum J. Nanoindentation of chromium zigzag thin films sputter deposited. Surf Coatings Technol 2005;200:269–72.
[34] Sit J, Vick D, Robbie K, Brett M. Thin film microstructure control using glancing angle deposition by sputtering. J Mater Res 1999;14:1197–9.
[35] Besnard A, Martin N, Sthal F, Carpentier L, Rauch J-Y. Metal-to-dielectric transition induced by annealing of oriented titanium thin films. Funct Mater Lett 2013;6.
[36] Li Z, Xing L, Zhang Z. Photocatalytic properties of columnar nanostructured TiO. Adv Mater Sci Eng 2012;2012.
[37] Michalcik Z, Horakova M, Spatenka P, Klementova S, Zlamal M, Martin N. Photocatalytic activity of nanostructured titanium dioxide thin films. Int J Photoenergy 2012;2012.
[38] In S-I, Almtoft KP, Lee H, Andersen IH, Qin D, Bao N, et al. Low temperature synthesis of transparent, vertically aligned anatase TiO_2 nanowire arrays: application to dye sensitized solar cells. Bull Korean Chem Soc 2012;33:1989.
[39] Grätzel M. Photoelectrochemical cells. Nature 2001;414:338–44.
[40] Kalyanasundaram K, Grätzel M. Applications of functionalized transition metal complexes in photonic and optoelectronic devices. Coord Chem Rev 1998;177:347–414.
[41] Schwartz BJ. Conjugated polymers as molecular materials: how chain conformation and film morphology influence energy transfer and interchain interactions. Annu Rev Phys Chem 2003;54:141–72.
[42] Feast W, Tsibouklis J, Pouwer K, Groenendaal L, Meijer E. Synthesis, processing and material properties of conjugated polymers. Polymer 1996;37:5017–47.
[43] Marrocchi A, Lanari D, Facchetti A, Vaccaro L. Poly (3-hexylthiophene): synthetic methodologies and properties in bulk heterojunction solar cells. Energy Environ Sci 2012;5:8457–74.
[44] Stefan MC, Bhatt MP, Sista P, Magurudeniya HD. Grignard metathesis (GRIM) polymerization for the synthesis of conjugated block copolymers containing regioregular poly (3-hexylthiophene). Polym Chem 2012;3:1693–701.
[45] Guo X, Baumgarten M, Müllen K. Designing π-conjugated polymers for organic electronics. Prog Polym Sci 2013;38:1832–908.
[46] Boon F, Thomas A, Clavel G, Moerman D, De Winter J, Laurencin D, et al. Synthesis and characterization of carboxystyryl end-functionalized poly (3-hexylthiophene)/TiO_2 hybrids in view of photovoltaic applications. Synth Met 2012;162:1615–22.
[47] Loewe RS, Ewbank PC, Liu J, Zhai L, McCullough RD. Regioregular, head-to-tail coupled poly (3-alkylthiophenes) made easy by the GRIM method: investigation of the reaction and the origin of regioselectivity. Macromolecules 2001;34:4324–33.
[48] Yokoyama A, Miyakoshi R, Yokozawa T. Chain-growth polymerization for poly (3-hexylthiophene) with a defined molecular weight and a low polydispersity. Macromolecules 2004;37:1169–71.
[49] Wu S, Huang L, Tian H, Geng Y, Wang F. LiCl-promoted chain growth Kumada catalyst-transfer polycondensation of the “reversed” thiophene monomer. Macromolecules 2011;44:7558–67.
[50] Miyakoshi R, Yokoyama A, Yokozawa T. Synthesis of Poly (3-hexylthiophene) with a narrower polydispersity. Macromol Rapid Commun 2004;25:1663–6.
[51] Nguyen HT, Coulembier O, De Winter J, Gerbaux P, Crispin X, Dubois P. Novel regioregular poly (3-hexylthiophene)-based polycationic block copolymers. Polym Bull 2011;66:51–64.
[52] Surin M, Coulembier O, Tran K, Winter JD, Leclère P, Gerbaux P, et al. Regioregular poly (3-hexylthiophene)-poly (ε-caprolactone) block copolymers: controlled synthesis, microscopic morphology, and charge transport properties. Org Electron 2010;11:767–74.
[53] Lub J, Ferrer A, Larossa C, Malo B. Synthesis and properties of chiral stilbene diacrylates. Liq Cryst 2003;30:1207–18.
[54] Thornton JA. Influence of apparatus geometry and deposition conditions on the structure and topography of thick sputtered coatings. J Vac Sci Technol 1974;11:666–70.
[55] Thornton JA. The microstructure of sputter-deposited coatings. J Vac Sci Technol A 1986;4:3059–65.
[56] Müller K-H. Ion-beam-induced epitaxial vapor-phase growth: a molecular-dynamics study. Phys Rev B 1987;35:7906.
[57] Fleischauer MD, Sorge JB, Joseph RA, Brett MJ. Enhanced control of porous thin film morphology via ion bombardment. In: MRS Proceedings. Cambridge Univ Press; 2006. pp. 0960-N0901-0903.
[58] Sorge J, Brett M. Film morphology modification in ion-assisted glancing angle deposition. Thin Solid Films 2010;519:1356–60.
[59] Thamaphat K, Limsuwan P, Ngotawornchai B. Phase characterization of TiO2 powder by XRD and TEM. Kasetsart J (Nat. Sci.) 2008;42:357–61.
[60] Löbl P, Huppertz M, Mergel D. Nucleation and growth in TiO2 films prepared by sputtering and evaporation. Thin Solid Films 1994;251:72–9.
[61] Krug J. Islands, mounds, and atoms: patterns and processes in crystal growth far from equilibrium. Nelson Thornes; 2004.
[62] Zhang Y, Ma X, Chen P, Yang D. Effect of the substrate temperature on the crystallization of TiO_2 films prepared by DC reactive magnetron sputtering. J Cryst Growth 2007;300:551–4.
[63] Wong M-S, Lee M-F, Chen C-L, Huang C-H. Vapor deposited sculptured nanoporous titania films by glancing angle deposition for efficiency enhancement in dye-sensitized solar cells. Thin Solid Films 2010;519:1717–22.
[64] Patzig C, Karabacak T, Fuhrmann B, Rauschenbach B. Glancing angle sputter deposited nanostructures on rotating substrates: experiments and simulations. J Appl Phys 2008;104:094318.